SELF-SUPERVISED MONOCULAR DEPTH ESTIMATION ROBUST TO REFLECTIVE SURFACE LEVERAGED BY TRIPLET MINING

Anonymous authors
Paper under double-blind review

ABSTRACT

Self-supervised monocular depth estimation (SSMDE) aims to predict the dense depth map of a monocular image, by learning depth from RGB image sequences, eliminating the need for ground-truth depth labels. Although this approach simplifies data acquisition compared to supervised methods, it struggles with reflective surfaces, as they violate the assumptions of Lambertian reflectance, leading to inaccurate training on such surfaces. To tackle this problem, we propose a novel training strategy for an SSMDE by leveraging triplet mining to pinpoint reflective regions at the pixel level, guided by the camera geometry between different viewpoints. The proposed reflection-aware triplet mining loss specifically penalizes the inappropriate photometric error minimization on the localized reflective regions while preserving depth accuracy on non-reflective areas. We also incorporate a reflection-aware knowledge distillation method that enables a student model to selectively learn the pixel-level knowledge from reflective and non-reflective regions. This results in robust depth estimation across areas. Evaluation results on multiple datasets demonstrate that our method effectively enhances depth quality on reflective surfaces and outperforms state-of-the-art SSMDE baselines.

1 INTRODUCTION

Self-supervised monocular depth estimation (SSMDE) (Godard et al., 2019) is a task that learns depth solely from a continuous RGB image sequence without needing corresponding ground-truth depth maps for each frame in a video. This approach significantly simplifies data acquisition compared to traditional supervised methods (Fu et al., 2018; Lee et al., 2019; Bhat et al., 2021), which often involve high costs for annotation. As such, many SSMDE studies (Godard et al., 2019; Zhou et al., 2017; Garg et al., 2016; Guizilini et al., 2020) have explored its viability as a mainstay for applications such as autonomous driving, highlighting its potential in outdoor environments.

Despite its advantages, SSMDE typically challenges in accurate depth estimation on non-Lambertian surfaces such as mirrors, transparent objects, and specular surfaces. This difficulty primarily arises from the assumption of Lambertian reflectance (Basri & Jacobs, 2003) embedded in most SSMDE methods. As illustrated in Figure 1, these non-Lambertian surfaces violate the photometric constancy principle, which posits that the color and brightness of a point should appear constant across different images (Godard et al., 2017). This violation leads to incorrect depth training, particularly on non-Lambertian surfaces. Consequently, this issue manifests in a phenomenon known as the "black-hole effect" (Shi et al., 2023), where the model erroneously predicts depths that are greater than the actual surface depth in areas with specular reflections. This effect is a prevalent challenge across various reflective surfaces, significantly impacting the performance and reliability of SSMDE systems.

Recent advancements (Costanzino et al., 2023; Shi et al., 2023) attempt to tackle these challenges by utilizing training strategies that involve generating pseudo-labels through inpainting (Costanzino et al., 2023) or reconstructing 3D meshes (Shi et al., 2023). However, these methods still rely on extra labels such as segmentation mask annotations (Costanzino et al., 2023) or use auxiliary methods that have excessive computational costs such as ensemble-based uncertainty algorithms (Shi et al., 2023), TSDF-fusion (Newcombe et al., 2011) and mesh rendering (Matl, 2019).

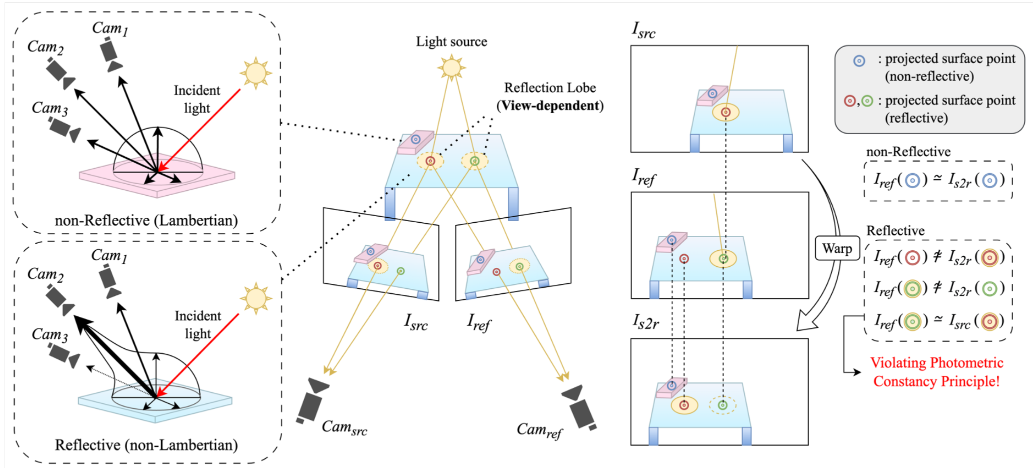

Figure 1: Photometric constancy violation on reflective surfaces. The projected non-reflective surface point (denoted as ⊙) satisfies the photometric constancy so the model can obtain the accurate depth by photometric error minimization. On the other hand, projected reflective surface point (denoted as ⊙,⊙) violates the photometric constancy, resulting in wrong disparity by photometric error minimization. This figure depicts a scenario where the relative positions of the cameras shift horizontally, akin to rectified stereo, to simplify the illustration.

To address these issues, we propose a novel training strategy called "*reflection-aware triplet mining*" that enhances the performance of SSMDEs by leveraging the triplet mining (Schroff et al., 2015). The underlying principle of our approach is that reflective areas, such as mirror light sources or objects, exhibit disparities corresponding to the reflected object rather than the actual surface as illustrated in Figure 1. While non-reflective areas exhibit photometric error due to the difference in camera views from two different perspectives (*e.g.*, source and reference views), reflective areas have abnormally low photometric error between the two views due to the low disparity of reflected objects. Accordingly, our approach treats views from the same camera coordinates as positive pairs and those from different coordinates as negative pairs, as illustrated in Figure 2. Our method aims to minimize the conventional photometric error between positive pairs while maximizing it between negative pairs. This approach effectively neutralizes the impact of contaminated gradients in reflective regions, thereby significantly improving accuracy on these regions.

Moreover, we introduce a "*reflection-aware knowledge distillation*" approach to keep the high-frequency details in the predicted depth for non-reflective regions inspired by previous works (Shi et al., 2023). In this method, the student network is trained by distilling knowledge from two distinct SSMDE networks. The first utilizes the proposed triplet loss, providing robustness against reflective areas, while the second employs solely photometric minimization loss, adept at preserving high-frequency details that contribute to the perceptual quality and visual fidelity of the depth map. This hybrid training strategy effectively combines the strengths of both training methods, creating a more versatile and effective depth estimation framework. By leveraging the unique capabilities of each model, the student network can achieve a more comprehensive understanding of depth across various surface conditions.

Our method is broadly applicable to general SSMDE frameworks that rely on photometric error minimization. We validate our method on three well-known SSMDE networks (Godard et al., 2019; Lyu et al., 2021; Zhao et al., 2022) across three public datasets (Dai et al., 2017; Shotton et al., 2013; Ramirez et al., 2023) featuring reflective objects and surfaces. The results demonstrate that our method significantly improves depth prediction accuracy on reflective surfaces while preserving performance on non-reflective surfaces. Our main contributions are fourfold as follows:

1. We propose a new *reflection-aware triplet mining loss* that significantly enhances the accuracy on reflective surfaces and can be easily integrated into general SSMDE frameworks.

2. We introduce *reflection-aware knowledge distillation* to improve the overall accuracy on reflective surfaces while preserving high-frequency details on non-reflective surfaces.
3. To the best of our knowledge, our strategy represents the first end-to-end method specifically designed to enhance the performances of SSMDE on reflective surfaces.
4. The proposed method outperforms the existing self-supervised training method and shows comparable results against 3D information distillation methods on various indoor depth benchmarks.

2 Related Work

2.1 Self-supervised monocular depth estimation

Self-supervised Monocular Depth Estimation (SSMDE) is a task that estimates a depth map from a single image without a ground truth depth map. This approach significantly simplifies the process of data acquisition, making it scalable for a wide variety of datasets. SfMLearner (Zhou et al., 2017) introduces a pioneering framework for self-supervised depth map estimation, which simultaneously learns depth maps for the input image and pose parameters from sequential views. Monodepth2 (Godard et al., 2019) proposes a masking scheme and minimum reprojection loss to filter out the regions that violate photometric inconstancy, such as moving objects and occluded regions. Subsequent methods (Zhou et al., 2021; Guizilini et al., 2020; Lyu et al., 2021) have been refined, effectively integrating features of different resolutions based on established constraints. With the introduction of ViT (Dosovitskiy et al., 2020), the field of SSMDE has begun to incorporate transformer backbones. Monoformer (Bae et al., 2023b) and MonoViT (Zhao et al., 2022) have emerged, utilizing hybrid networks of CNN and transformers to adeptly merge local and global features.

2.2 Generalization of monocular depth estimation

Recent research has expanded to consider factors such as the impact of weather variations (Saunders et al., 2023; Gasperini et al., 2023), the differences in inference capabilities between CNNs and Transformers (Bae et al., 2023a), the robustness of SSMDEs against various types of data corruption (Kong et al., 2024), and methods for accurately modeling transparent and mirrored surfaces, which are typically non-Lambertian (Costanzino et al., 2023). In addition, the 3D Distillation (Shi et al., 2023) addresses a critical flaw in traditional SSMDEs: the photometric constancy principle used in applying photometric consistency loss may not hold for non-Lambertian surfaces encountered in real-world scenarios, resulting in SSMDE models producing unreliable and low-quality depth estimates for reflective surfaces. To counter this problem, 3D Distillation leverages the 3D mesh rendering function along with ensemble uncertainty to localize the reflective surfaces and refine the inaccurate depth on these regions.

2.3 Deep metric learning

Deep metric learning (Chen et al., 2020; Chen & He, 2021; Khosla et al., 2020) seeks to develop an effective distance measure between data points. These methods strive to minimize the distance between samples of the same class while maximizing it between samples from different classes. While traditionally focused on classification tasks, where positive and negative pairs are defined based on class similarity, recent studies (Spurr et al., 2021; Wang et al., 2022; Zha et al., 2024) have expanded the application of deep metric learning to regression contexts. Particularly in the context of depth estimation, deep metric learning has demonstrated versatility beyond simple augmentation-based consistency. It has been applied to enhance accuracy through contrasting depth distributions (Fan et al., 2023; Choi et al., 2024) and addressing issues such as edge fattening (Chen et al., 2023). In this paper, we utilize the triplet mining scheme, initially popularized by Schroff et al. (2015), to enhance recognition accuracy, specifically focusing on improving performance on reflective surfaces.

3 Method

Our method aims to enhance depth prediction accuracy on reflective surfaces by strategically penalizing the inappropriate photometric error minimization between the view-synthesized image and the reference image. In Section 3.1, we discuss the photometric constancy principle, which posits that correctly minimizing photometric error is crucial for accurately determining depth (Section 3.1.1). We also provide an overview of the standard training strategies employed in SSMDE frameworks (Section 3.1.2). In Section 3.2, we detail the three components of our training strategy: reflective region localization (Section 3.2.1), reflection-aware triplet mining loss (Section 3.2.2), and reflection-aware knowledge distillation (Section 3.2.3).

3.1 PRELIMINARY

3.1.1 PHOTOMETRIC CONSTANCY PRINCIPLE

The photometric constancy principle is foundational in SSMDE frameworks, positing that surfaces exhibit uniform reflectance (*i.e.*, Lambertian reflectance) from all viewing angles. A surface adheres to this principle if its color and luminance observed through a camera remain constant, regardless of the camera's viewing angle. By leveraging this property, depth and pose can be accurately estimated by minimizing the photometric error between the view-synthesized image and the reference image, as described in Equation 3. However, real-world scenes rarely adhere strictly to this principle. Non-Lambertian surfaces, such as specular reflections from light sources or mirrored objects, are prevalent, leading to violations of photometric constancy. These deviations result in significant errors when attempting to minimize photometric error, thus compromising the effectiveness of depth estimation methods based on these assumptions.

3.1.2 TRAINING STRATEGY OF GENERAL SSMDE FRAMEWORK

The objective of SSMDE is to predict a per-pixel basis depth map $\mathbf{D}_{ref}$ of a reference image $\mathbf{I}_{ref}$ given the reference image itself, a source image $\mathbf{I}_{src}$ (or source images) and their camera intrinsics $\boldsymbol{K}$. The framework consists of a depth network $\mathcal{F}_\theta(\cdot)$, and a pose network $\mathcal{G}_\phi(\cdot,\cdot)$ to respectively estimate the depth of the reference image $\mathbf{D}_{ref}$, and the relative pose $[\boldsymbol{R}|\boldsymbol{t}]_{r2s}$ as follows:

$$\mathbf{D}_{ref} = \mathcal{F}_\theta(\mathbf{I}_{ref}), \qquad \mathcal{F}_\theta : \mathbb{R}^{3\times h\times w} \rightarrow \mathbb{R}^{1\times h\times w}, \tag{1}$$

$$[\boldsymbol{R}|\boldsymbol{t}]_{r2s} = \mathcal{G}_\phi(\mathbf{I}_{src}, \mathbf{I}_{ref}), \quad \mathcal{G}_\phi : \mathbb{R}^{2\times 3\times h\times w} \rightarrow \mathbb{R}^{3\times 4}, \tag{2}$$

where (h, w) represent the spatial resolution of $\mathbf{I}_{ref}$. Using the obtained relative pose $[\boldsymbol{R}|\boldsymbol{t}]_{r2s}$, and depth map $\mathbf{D}_{ref}$, the source image $\mathbf{I}_{src}$ is warped into the reference coordinates, generating the view-synthesized image $\mathbf{I}_{s2r}$ as follows:

$$(\mathbf{I}_{s2r})_{:,u,v} = \mathbf{I}_{src}(\langle \boldsymbol{K}[\boldsymbol{R}|\boldsymbol{t}]_{r2s}(\mathbf{D}_{ref})_{:,u,v}\boldsymbol{K}^{-1}[u, v, 1]^T\rangle), \tag{3}$$

where (u, v) represent the image coordinates and $\langle\cdot\rangle$ is the projection function that maps homogeneous coordinates to cartesian coordinates. By the photometric constancy principle detailed in Section 3.1.1, the synthesized image $\mathbf{I}_{s2r}$ should exhibit the same colors and luminances as the reference image on a pixel-by-pixel basis. Consequently, the model can determine the accurate depth and pose by minimizing the photometric errors, $\mathcal{P}(\cdot,\cdot)$, between $\mathbf{I}_{s2r}$ and $\mathbf{I}_{ref}$ as follows:

$$\begin{gathered}\mathcal{P}(\mathbf{I}_{s2r}, \mathbf{I}_{ref}) = \mathbf{M} \odot \left(\alpha_1 \frac{1 - \mathcal{S}(\mathbf{I}_{ref}, \mathbf{I}_{s2r})}{2} + \alpha_2 ||\mathbf{I}_{ref} - \mathbf{I}_{s2r}||_1\right), \\ \mathcal{P} : \mathbb{R}^{2\times 3\times h\times w} \rightarrow \mathbb{R}^{1\times h\times w}, \quad \mathcal{S} : \mathbb{R}^{2\times 3\times h\times w} \rightarrow \mathbb{R}^{1\times h\times w},\end{gathered} \tag{4}$$

where $\mathcal{S}(\cdot,\cdot)$ is the mixture of structural similarity index (Wang et al., 2004), and $\mathbf{M}$ is the principled mask (Godard et al., 2019) to prevent the backpropagation of corrupted gradients, caused by anomalies like moving objects in the scene. The weights α_1 and α_2 serve as balance terms between two losses, and $\odot$ represents the element-wise multiplication operator. However, if the surface does not conform to the principle of photometric constancy, minimizing photometric errors on such reflective surfaces can lead to significant inaccuracies in the estimated depth.

3.2 METHODOLOGY

3.2.1 REFLECTIVE REGION LOCALIZATION

The photometric error, as calculated through Equation 4 between I_{s2r} and I_{ref} tends to be smaller in non-reflective regions. This is because these areas reflect consistent colors and luminances irrespective of the viewing direction, adhering to the photometric constancy principle. On the other

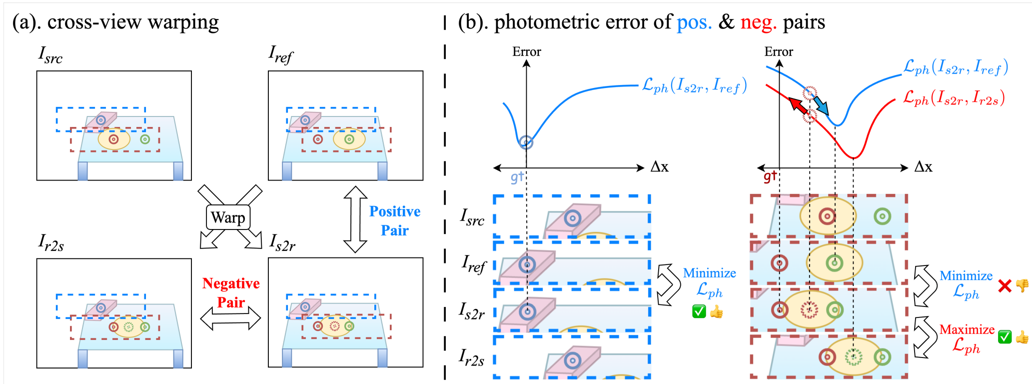

Figure 2: The effect of the proposed method on reflective/non-reflective surfaces. (◎/◎,◎) imply the projected non-reflective/reflective surface points, respectively, and (◎, ◎) denotes the location of reflection lobe in view-synthesized image coordinate. Our proposed method cancels out the wrong photometric error minimization in reflection areas by contrasting the negative pair samples.

hand, reflective regions, which violate the photometric constancy principle, exhibit abnormally low disparities due to the additional distance from the reflected light source. Consequently, as illustrated in Figure 2, reflection lobes from different images appear relatively closer in image coordinates, resulting in reduced photometric errors in the RGB images of two different viewpoints.

This characteristic is crucial for isolating reflective regions within the spatial dimension of the image. To capitalize on this, we first generate cross-view synthesized images I_{s2r}, I_{r2s} in a manner similar to the process outlined in Equation 3:

$$(\mathbf{I}_{s2r})_{:,u,v} = \mathbf{I}_{src}(\langle \boldsymbol{K}[\boldsymbol{R}|\boldsymbol{t}]_{r2s}(\mathbf{D}_{ref})_{:,u,v}\boldsymbol{K}^{-1}[u, v, 1]^T\rangle), \tag{5}$$

$$(\mathbf{I}_{r2s})_{:,u,v} = \mathbf{I}_{ref}(\langle \boldsymbol{K}[\boldsymbol{R}|\boldsymbol{t}]_{s2r}(\mathbf{D}_{src})_{:,u,v}\boldsymbol{K}^{-1}[u, v, 1]^T\rangle), \tag{6}$$

where the relative pose $[\boldsymbol{R}|\boldsymbol{t}]_{s2r}$ can be obtained by computing the inverse of the predicted pose $[\boldsymbol{R}|\boldsymbol{t}]_{s2r}$, and $\mathbf{D}_{src}$ is predicted depth from $\mathbf{I}_{src}$, following a procedure similar to Equation 1. Utilizing these synthesized cross-view images, we compute two photometric errors to measure discrepancies between image pairs as follows:

$$\mathbf{E}^+ = \mathcal{P}(\mathbf{I}_{s2r}, \mathbf{I}_{ref}), \quad \mathbf{E}^- = \mathcal{P}(\mathbf{I}_{s2r}, \mathbf{I}_{r2s}). \tag{7}$$

The first error, $\mathbf{E}^+$, quantifies discrepancies between images taken from the same viewpoint $(\mathbf{I}_{s2r}, \mathbf{I}_{ref})$. This error is minimized when depth and pose are accurately estimated on non-reflective surfaces. Conversely, the second error, $\mathbf{E}^-$, measures discrepancies between images from different viewpoints $(\mathbf{I}_{s2r}, \mathbf{I}_{r2s})$. In general, the expected photometric error for $\mathbf{E}^-$ should be substantial due to the different camera coordinate systems. However, on reflective surfaces, the variations in light reflection may result in a reduced photometric error. Based on these observations, we identify pixel-level reflective regions $\mathbf{M}_r \in \mathbb{R}^{1\times h\times w}$ as follows:

$$(\mathbf{M}_r)_{:,u,v} = \begin{cases} 1, & \text{if } (\mathbf{E}^-)_{:,u,v} - (\mathbf{E}^+)_{:,u,v} \leq \delta, \\ 0, & \text{else,} \end{cases} \tag{8}$$

where δ is a certain margin that represents the minimum significant photometric difference required to distinguish between the two surface types, where a value of 1 corresponds to a reflective pixel and 0 to a non-reflective pixel, respectively. This method effectively utilizes discrepancies in photometric errors to distinguish between reflective and non-reflective surfaces, providing a precise mapping of surface properties within the image. (refer to Section D in the supplementary materials.)

3.2.2 Reflection-aware triplet mining loss

We introduce the reflection-aware triplet mining loss, $\mathcal{L}_{tri}$, which addresses the limitations of using $\mathbf{E}^+$ alone in environments where reflections disrupt depth accuracy. In reflective regions, simply minimizing $\mathbf{E}^+$ does not effectively discern between real and reflected disparities. To counteract this, we assert that $\mathbf{E}^-$ should be significantly greater than $\mathbf{E}^+$. This approach is inspired by triplet mining techniques that aim to minimize the distance within positive pairs and maximize it within negative pairs, enhancing the model's ability to distinguish between reflective and non-reflective surfaces. To implement this, we formulate the reflection-aware triplet mining loss as follows:

$$\mathcal{L}_{tri}(\mathbf{I}_{ref}, \mathbf{I}_{s2r}, \mathbf{I}_{r2s}) = \mathbf{M}_r \odot (\mathbf{E}^+ - \mathbf{E}^- + \delta)_{hinge} + \big(1 - \mathbf{M}_r\big) \odot \mathbf{E}^+, \tag{9}$$

where $(\cdot)_{hinge}$ is the hinge loss function described in Hearst et al. (1998). In this configuration, the reflection-aware triplet mining loss is applied specifically to regions identified as reflective. For non-reflective regions, where reflections do not disrupt photometric assessments, we apply the photometric loss $\mathbf{E}^+$ as it reliably reflects photometric consistency. This differentiation allows the model to address the unique challenges presented by each type of region effectively.

As illustrated in Figure 2, this strategy involves not only penalizing the minimization of $\mathbf{E}^+$ but also actively maximizing $\mathbf{E}^-$. This method effectively counteracts the contaminated gradients typically found in reflective regions. By adjusting the balance between $\mathbf{E}^+$ and $\mathbf{E}^-$ based on the presence of reflective surfaces, our method not only improves depth estimation in complex scenarios but also ensures robust performance against the challenges posed by reflective surfaces. This comprehensive approach results in a model that accurately reflects the true topography of both reflective and non-reflective environments.

3.2.3 Reflection-aware knowledge distillation

The proposed end-to-end training scheme described in Section 3.2.2 effectively handles the depth estimation on both reflective and non-reflective surfaces. To further refine depth estimation quality, we introduce a reflection-aware knowledge distillation strategy inspired by the fusion techniques discussed in Shi et al. (2023), aimed at retaining high-frequency details in depth prediction.

Our approach begins by training two separate SSMDE networks. The first is trained using our reflection-aware triplet mining loss, $\mathcal{L}_{tri}$, as defined in Equation 9, and the second employs the conventional photometric loss, $\mathbf{E}^+$. From these models, we generate two types of depth maps: $\mathbf{D}_{tri}$, derived from the reflection-aware model, and $\mathbf{D}_{ori}$, obtained from the model trained with conventional photometric loss. We then merge these depth maps into a single pseudo depth map $\mathbf{D}_{pse}$ utilizing a reflective region mask $\mathbf{M}_r$. This mask facilitates the adaptive fusing of depth information from both teacher models based on the presence of reflective properties in the image. The pseudo depth map generation and distillation process is detailed in the following equation:

$$\mathcal{L}_{rkd}(\hat{\mathbf{D}}, \mathbf{D}_{pse}) = |\log \hat{\mathbf{D}} - \log \mathbf{D}_{pse}|, \text{ where } \mathbf{D}_{pse} = \mathbf{M}_r \odot \mathbf{D}_{tri} + (1 - \mathbf{M}_r) \odot \mathbf{D}_{ori}, \tag{10}$$

where $\hat{\mathbf{D}}$ represents the depth predicted by the student model. It is important to note that the student model and the two teacher models share the same network architecture as the general SSMDEs. This structured training approach not only addresses the specific challenges posed by reflective surfaces but also ensures that the high-frequency detail is not lost, thus achieving a balanced and accurate depth prediction across different surface types.

4 Experiments

Datasets. ***ScanNet (v2)*** (Dai et al., 2017) is a comprehensive indoor RGB-D video dataset comprising 2.7 million images across 1,216 interior scene sequences. Traditionally, this dataset has been pivotal for evaluating multi-view stereo (Im et al., 2019; Bae et al., 2022) and scene reconstruction applications (Murez et al., 2020; Zhou et al., 2024). ***7-Scenes*** (Shotton et al., 2013) is a challenging RGB-D dataset captured in indoor scenes with a similar distribution to *ScanNet* but dominated by non-reflective surfaces. We follow the evaluation protocol of Long et al. (2021); Bae et al. (2022) to demonstrate the cross-dataset generalization performances. ***Booster*** (Ramirez et al., 2023) includes a variety of non-Lambertian objects within indoor settings, such as transparent basins, mirrors, and specular surfaces. Following the Costanzino et al. (2023), we use the training split as our test set, which showcases our method's adaptability to more complex scenes.

Training scenario. In the work of 3D distillation (Shi et al., 2023), the ScanNet dataset has been further segmented into ScanNet-Reflection and ScanNet-NoReflection subsets based on the presence of reflective objects within the scenes. This subdivision results in a ScanNet-Reflection dataset

Table 1: Main results on the ScanNet-Reflection Test and Validation sets.

	Backbone	Training Scheme	Method	Abs Rel ↓	Sq Rel ↓	RMSE ↓	RMSE log ↓	$\delta < 1.25$ ↑	$\delta < 1.25^2$ ↑	$\delta < 1.25^3$ ↑
ScanNet-Reflection Test	Monodepth2	End-to-End	Self-Supervised	0.181	0.160	0.521	0.221	0.758	0.932	0.976
			Ours	**0.157**	**0.096**	**0.468**	**0.201**	**0.762**	**0.949**	**0.988**
		Multi-Stage	Self-Teaching	0.179	0.146	0.502	0.218	0.750	0.938	0.980
			3D Distillation	0.156	0.096	0.459	0.195	0.766	0.945	0.988
			Ours†	**0.150**	**0.087**	**0.446**	**0.192**	**0.777**	**0.955**	**0.990**
	HRDepth	End-to-End	Self-Supervised	0.182	0.168	0.530	0.225	0.749	0.937	0.979
			Ours	**0.157**	**0.098**	**0.470**	**0.201**	**0.763**	**0.952**	**0.989**
		Multi-Stage	Self-Teaching	0.175	0.145	0.492	0.215	0.757	0.936	0.982
			3D Distillation	0.152	**0.089**	0.451	**0.190**	0.771	**0.956**	**0.990**
			Ours†	**0.150**	0.092	**0.434**	0.192	**0.780**	0.950	0.988
	MonoViT	End-to-End	Self-Supervised	0.154	0.129	0.458	0.197	0.822	0.955	0.979
			Ours	**0.136**	**0.087**	**0.414**	**0.178**	**0.831**	**0.967**	**0.988**
		Multi-Stage	Self-Teaching	0.151	0.130	0.439	0.191	0.837	0.950	0.978
			3D Distillation	0.127	**0.069**	**0.379**	**0.162**	0.846	0.961	**0.992**
			Ours†	**0.126**	0.074	0.395	0.167	**0.854**	**0.969**	0.990
ScanNet-Reflection Validation	Monodepth2	End-to-End	Self-Supervised	0.206	0.227	0.584	0.246	0.750	0.912	0.961
			Ours	**0.166**	**0.125**	**0.492**	**0.209**	**0.763**	**0.934**	**0.981**
		Multi-Stage	Self-Teaching	0.192	0.188	0.548	0.233	0.764	0.920	0.967
			3D Distillation	0.156	**0.093**	**0.442**	**0.191**	0.786	0.943	**0.987**
			Ours†	**0.151**	0.105	0.454	0.193	**0.796**	**0.944**	0.985
	HRDepth	End-to-End	Self-Supervised	0.213	0.244	0.605	0.255	0.741	0.906	0.961
			Ours	**0.167**	**0.127**	**0.496**	**0.210**	**0.770**	**0.937**	**0.982**
		Multi-Stage	Self-Teaching	0.202	0.208	0.565	0.243	0.756	0.914	0.964
			3D Distillation	0.153	**0.090**	**0.430**	**0.188**	0.789	0.948	**0.989**
			Ours†	**0.151**	0.104	0.450	0.192	**0.800**	**0.949**	0.987
	MonoViT	End-to-End	Self-Supervised	0.179	0.206	0.557	0.227	0.819	0.930	0.963
			Ours	**0.139**	**0.107**	**0.452**	**0.183**	**0.836**	**0.954**	**0.984**
		Multi-Stage	Self-Teaching	0.176	0.195	0.537	0.224	0.823	0.930	0.963
			3D Distillation	**0.126**	**0.068**	**0.367**	**0.159**	**0.851**	**0.965**	**0.991**
			Ours†	0.130	0.091	0.420	0.173	**0.851**	0.960	0.987

consisting of 45,539 training, 439 validation, and 121 testing samples. Additionally, a ScanNet-NoReflection validation set comprising 1,012 samples evaluates the model's generalization when trained in reflective environments. Aligning with these methodologies, the training process leverages the ScanNet-Reflection train set to simulate real-world scenarios involving reflective surfaces.

Evaluation. For quantitative evaluations, we employ standard metrics from the depth estimation literature (Eigen et al., 2014; Geiger et al., 2012). We differentiate our training approaches into end-to-end and multi-stage (distillation) strategies to effectively assess the models. The model trained solely using reflection-aware triplet mining loss $\mathcal{L}_{tri}$, referred to as "*Ours*", and another utilizing the proposed distillation method $\mathcal{L}_{rkd}$, referred to as "*Ours*†", are evaluated under their respective conditions. We compare these against both end-to-end and multi-stage baselines across three sets: ScanNet-Reflection $\{$Test, Validation$\}$ sets, and ScanNet-NoReflection Validation set. To underline the cross-dataset generalizability of our methods, we also perform zero-shot evaluations on the 7-Scenes and Booster.

Implementation details. Our experiments incorporate three leading architectures in SSMDE: ***Monodepth2*** (Godard et al., 2019), ***HRDepth*** (Lyu et al., 2021), and ***MonoViT*** (Zhao et al., 2022), which have demonstrated exceptional performance in previous studies. Each backbone is trained by different training schemes, including Self-Supervised (Godard et al., 2019), Self-Teaching (Poggi et al., 2020), and 3D Distillation (Shi et al., 2023), to compare with our method. To align closely with 3D Distillation, all training particulars follow their documented conditions, with adaptations only in our proposed training strategy. Specifically, the models are trained using the reflection triplet split introduced in 3D Distillation. To finely tune the margin δ across positive and negative pairs, it is adaptively selected based on the difference between the first quartile (Q1) of $\mathbf{E}^+$ and the third quartile (Q3) of $\mathbf{E}^-$.

4.1 Evaluation on reflection datasets

ScanNet-Reflection dataset. To demonstrate the effectiveness of the proposed method on reflective surfaces, we conduct a quantitative evaluation using the ScanNet-Reflection dataset. The eval-

Table 2: Main results on the ScanNet-NoReflection Validation set.

Backbone	Training Scheme	Method	Abs Rel ↓	Sq Rel ↓	RMSE ↓	RMSE log ↓	$\delta < 1.25$ ↑	$\delta < 1.25^2$ ↑	$\delta < 1.25^3$ ↑
Monodepth2	End-to-End	Self-Supervised	0.169	0.100	**0.395**	**0.206**	**0.759**	**0.932**	0.979
		Ours	**0.168**	**0.095**	**0.395**	0.208	0.751	0.931	**0.980**
	Multi-Stage	Self-Teaching	0.161	0.090	0.375	0.196	0.777	0.939	0.981
		3D Distillation	0.159	0.087	**0.373**	**0.195**	**0.779**	0.941	**0.983**
		Ours†	**0.157**	**0.085**	**0.373**	**0.195**	0.776	**0.942**	**0.983**
HRDepth	End-to-End	Self-Supervised	0.169	0.102	**0.388**	**0.202**	**0.766**	**0.933**	**0.980**
		Ours	**0.167**	**0.096**	0.389	0.204	0.764	**0.933**	0.979
	Multi-Stage	Self-Teaching	0.160	0.089	0.367	0.192	0.784	0.941	0.982
		3D Distillation	0.158	**0.086**	**0.365**	**0.190**	**0.786**	**0.942**	**0.983**
		Ours†	**0.157**	**0.086**	0.366	0.192	0.784	**0.942**	**0.983**
MonoViT	End-to-End	Self-Supervised	**0.140**	0.074	**0.333**	**0.171**	**0.829**	**0.952**	0.984
		Ours	0.141	**0.072**	0.338	0.174	0.823	**0.952**	**0.987**
	Multi-Stage	Self-Teaching	0.134	0.068	0.317	0.164	**0.840**	0.956	**0.987**
		3D Distillation	**0.133**	**0.065**	**0.311**	**0.162**	0.838	0.956	**0.987**
		Ours†	**0.133**	0.066	0.320	0.166	0.837	**0.957**	**0.987**

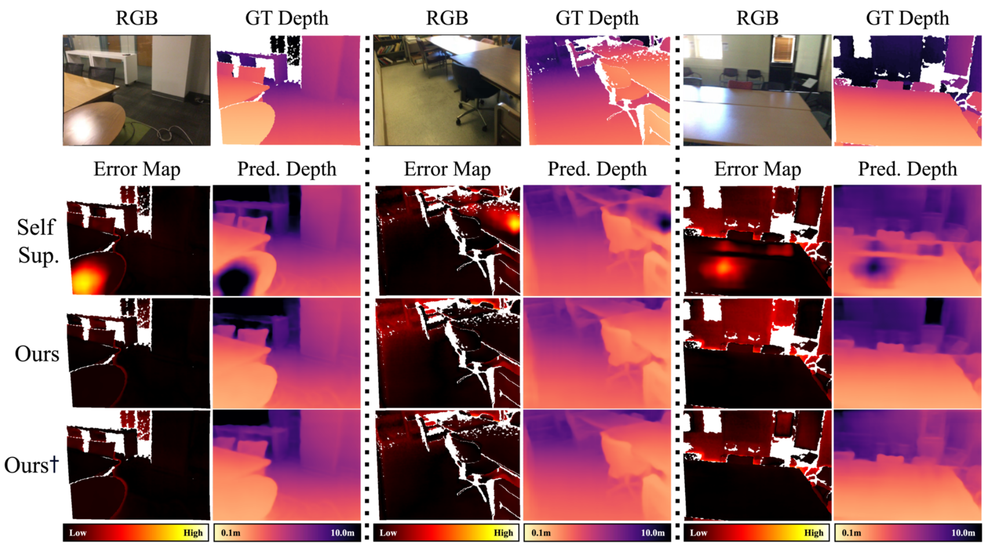

Figure 3: Qualitative results of the proposed methods on the ScanNet. We visualize the predicted depth of the Monodepth2 (Godard et al., 2019) trained by three different methods including the proposed method: Self-supervised, *Ours* and *Ours*†. Note that the error map represents the absolute difference between prediction and ground truth depth, normalized to between 0 and 255.

uations are divided into end-to-end and multi-stage methodologies. As depicted in Table 1, *Ours*, categorized under end-to-end training schemes, significantly outperforms self-supervised methods across all backbones, achieving an *Abs Rel* average increase of 12.90% in the test split and 21.12% in the validation split. Moreover, it is noteworthy that *Ours* shows a significant performance boost, with an average improvement of 10.75% over Self-Teaching across all metrics in both the test and validation splits, with only two exceptions in 42 metrics ($\delta < 1.25$ of Monodepth2 and MonoViT). This demonstrates that our reflection-aware triplet mining loss is effective in detecting reflective surfaces and encourages the model to obtain accurate depth on these surfaces as shown in Figure 3. Additionally, our multi-stage approach, which employs reflection-aware knowledge distillation (denoted as *Ours*†), delivers comparable results across all backbone models of 3D Distillation. Note that the proposed method does not require complex scene reconstruction procedures such as mesh rendering (Matl, 2019; Newcombe et al., 2011) or ensembles of multiple neural network models (Lakshminarayanan et al., 2017).

ScanNet-NoReflection dataset. Table 2 summarizes the results of a quantitative evaluation performed on the ScanNet-NoReflection dataset. This evaluation aims to measure the generalization

Table 3: Cross-dataset evaluation result on the 7-Scenes and booster datasets.

	Backbone	Method	Abs Rel ↓	Sq Rel ↓	RMSE ↓	RMSE log ↓	$\delta < 1.25$ ↑	$\delta < 1.25^2$ ↑	$\delta < 1.25^3$ ↑
7-Scenes	Monodepth2	Self-Supervised	0.210	0.130	0.445	0.248	0.656	0.906	0.974
		Ours	0.207	0.125	0.441	0.248	0.656	0.904	0.975
		Ours†	**0.198**	**0.110**	**0.415**	**0.238**	**0.667**	**0.911**	**0.980**
	HRDepth	Self-Supervised	0.193	0.115	0.421	0.231	0.682	0.921	0.982
		Ours	0.195	0.109	0.419	0.232	0.674	0.921	0.984
		Ours†	**0.183**	**0.096**	**0.389**	**0.219**	**0.706**	**0.931**	**0.986**
	MonoViT	Self-Supervised	0.173	0.093	0.365	0.201	0.752	0.945	0.988
		Ours	0.175	0.090	0.361	0.204	0.746	0.944	0.987
		Ours†	**0.162**	**0.077**	**0.335**	**0.191**	**0.776**	**0.951**	**0.989**
Booster	Monodepth2	Self-Supervised	0.520	0.429	0.601	0.444	0.305	0.591	0.827
		Ours	0.430	0.301	0.501	0.389	0.362	0.675	0.893
		Ours†	**0.419**	**0.288**	**0.487**	**0.381**	**0.370**	**0.678**	**0.897**
	HRDepth	Self-Supervised	0.495	0.391	0.559	0.426	0.307	0.611	0.852
		Ours	**0.414**	**0.276**	**0.482**	**0.379**	0.364	**0.680**	**0.907**
		Ours†	0.429	0.292	0.487	0.385	**0.366**	0.659	0.878
	MonoViT	Self-Supervised	0.418	0.327	0.504	0.374	**0.425**	0.679	0.888
		Ours	0.408	0.302	0.482	0.362	0.414	0.677	0.916
		Ours†	**0.375**	**0.249**	**0.440**	**0.337**	0.422	**0.734**	**0.944**

performance of models trained on datasets that include reflective surfaces. In an end-to-end training scheme, *Ours* achieves performance comparable to or within an acceptable margin of self-supervised methods. This confirms that our proposed reflection-aware triplet mining loss effectively prevents the incorrect back-propagation of the photometric loss gradient on reflective surfaces, as illustrated in Figure 2. Furthermore, the model trained by our reflection-aware knowledge distillation (*i.e.*, *Ours*†) shows a noticeable performance improvement, which is comparable performance to the 3D distillation method. These results suggest that extending our reflection-aware triplet mining loss to distillation techniques offers a straightforward yet effective strategy for managing reflective surfaces.

4.2 Cross-dataset generalizability

To demonstrate the generalization ability across different datasets, we conduct a zero-shot evaluation using 7-Scenes and Booster datasets. As shown in Table 3, our proposed methods (denoted as *Ours* and *Ours*†) consistently enhances performance. Specifically, across all backbone architectures and all metrics, *Ours*† improved by an average of 5.47% and 13.89% for the 7-Scenes and Booster datasets, respectively. Exceptionally, there is no significant difference between *Ours* and the self-supervised method on the 7-Scenes dataset. This may be attributed to the predominance of non-reflective surfaces in the 7-Scenes dataset, where our model, trained with the reflection-aware triplet mining loss, slightly loses high-frequency details on non-reflective surfaces. Conversely, the consistent performance improvement of *Ours*† across both reflective and non-reflective surfaces demonstrates the robust generalization capabilities of our method based on reflective region selection.

5 Conclusion

This paper addresses the intricate challenge of self-supervised monocular depth estimation on reflective surfaces. Our method employs a novel metric learning approach, centered around a reflection-aware triplet mining loss. This novel loss function significantly improves depth prediction accuracy by accurately identifying reflective regions on a per-pixel basis and effectively adjusting the minimization of photometric errors, which are typically problematic on reflective surfaces. It also preserves high-frequency details on non-reflective surfaces by selectively regulating photometric error minimization based on reflection region selection. Moreover, we introduce a reflection-aware knowledge distillation method, enabling a student model to enhance performance in both reflective and non-reflective surfaces. This method leverages the strengths of different teaching networks to produce a more robust and versatile student model. Experimental evaluations conducted on the indoor scene datasets demonstrate our method consistently enhances depth performance across various architectural frameworks. These results underscore the robustness and versatility of our approach, marking it as a valuable contribution to the field of self-supervised monocular depth estimation.

REFERENCES

Gwangbin Bae, Ignas Budvytis, and Roberto Cipolla. Multi-view depth estimation by fusing single-view depth probability with multi-view geometry. In *Proceedings of the IEEE/CVF Conference on Computer Vision and Pattern Recognition*, pp. 2842–2851, 2022.

Jinwoo Bae, Kyumin Hwang, and Sunghoon Im. A study on the generality of neural network structures for monocular depth estimation. *IEEE Transactions on Pattern Analysis and Machine Intelligence*, 2023a.

Jinwoo Bae, Sungho Moon, and Sunghoon Im. Deep digging into the generalization of self-supervised monocular depth estimation. In *Proceedings of the AAAI conference on artificial intelligence*, volume 37, pp. 187–196, 2023b.

Ronen Basri and David W Jacobs. Lambertian reflectance and linear subspaces. *IEEE transactions on pattern analysis and machine intelligence*, 25(2):218–233, 2003.

Shariq Farooq Bhat, Ibraheem Alhashim, and Peter Wonka. Adabins: Depth estimation using adaptive bins. In *Proceedings of the IEEE/CVF Conference on Computer Vision and Pattern Recognition*, pp. 4009–4018, 2021.

Ting Chen, Simon Kornblith, Mohammad Norouzi, and Geoffrey Hinton. A simple framework for contrastive learning of visual representations. In *ICML*, pp. 1597–1607. PMLR, 2020.

Xingyu Chen, Ruonan Zhang, Ji Jiang, Yan Wang, Ge Li, and Thomas H Li. Self-supervised monocular depth estimation: Solving the edge-fattening problem. In *Proceedings of the IEEE/CVF Winter Conference on Applications of Computer Vision*, pp. 5776–5786, 2023.

Xinlei Chen and Kaiming He. Exploring simple siamese representation learning. In *CVPR*, pp. 15750–15758, 2021.

Wonhyeok Choi, Mingyu Shin, and Sunghoon Im. Depth-discriminative metric learning for monocular 3d object detection. *Advances in Neural Information Processing Systems*, 36, 2024.

Alex Costanzino, Pierluigi Zama Ramirez, Matteo Poggi, Fabio Tosi, Stefano Mattoccia, and Luigi Di Stefano. Learning depth estimation for transparent and mirror surfaces. In *Proceedings of the IEEE/CVF International Conference on Computer Vision*, pp. 9244–9255, 2023.

Angela Dai, Angel X Chang, Manolis Savva, Maciej Halber, Thomas Funkhouser, and Matthias Nießner. Scannet: Richly-annotated 3d reconstructions of indoor scenes. In *Proceedings of the IEEE conference on computer vision and pattern recognition*, pp. 5828–5839, 2017.

Alexey Dosovitskiy, Lucas Beyer, Alexander Kolesnikov, Dirk Weissenborn, Xiaohua Zhai, Thomas Unterthiner, Mostafa Dehghani, Matthias Minderer, Georg Heigold, Sylvain Gelly, et al. An image is worth 16x16 words: Transformers for image recognition at scale. *arXiv preprint arXiv:2010.11929*, 2020.

David Eigen, Christian Puhrsch, and Rob Fergus. Depth map prediction from a single image using a multi-scale deep network. *Advances in neural information processing systems*, 27, 2014.

Rizhao Fan, Matteo Poggi, and Stefano Mattoccia. Contrastive learning for depth prediction. In *Proceedings of the IEEE/CVF Conference on Computer Vision and Pattern Recognition*, pp. 3225–3236, 2023.

Huan Fu, Mingming Gong, Chaohui Wang, Kayhan Batmanghelich, and Dacheng Tao. Deep ordinal regression network for monocular depth estimation. In *Proceedings of the IEEE conference on computer vision and pattern recognition*, pp. 2002–2011, 2018.

Ravi Garg, Vijay Kumar Bg, Gustavo Carneiro, and Ian Reid. Unsupervised cnn for single view depth estimation: Geometry to the rescue. In *Computer Vision–ECCV 2016: 14th European Conference, Amsterdam, The Netherlands, October 11-14, 2016, Proceedings, Part VIII 14*, pp. 740–756. Springer, 2016.

Stefano Gasperini, Nils Morbitzer, HyunJun Jung, Nassir Navab, and Federico Tombari. Robust monocular depth estimation under challenging conditions. In *Proceedings of the IEEE/CVF international conference on computer vision*, pp. 8177–8186, 2023.

A Geiger, M Nießner, M Pollefeys, C Rother, D Scharstein, AA Hassan, A Dai, K Honauer, J Janai, T Sattler, et al. Robust vision challenge. In *CVPR Workshop*, 2018.

Andreas Geiger, Philip Lenz, and Raquel Urtasun. Are we ready for autonomous driving? the kitti vision benchmark suite. In *2012 IEEE conference on computer vision and pattern recognition*, pp. 3354–3361. IEEE, 2012.

Clément Godard, Oisin Mac Aodha, and Gabriel J Brostow. Unsupervised monocular depth estimation with left-right consistency. In *Proceedings of the IEEE conference on computer vision and pattern recognition*, pp. 270–279, 2017.

Clément Godard, Oisin Mac Aodha, Michael Firman, and Gabriel J Brostow. Digging into self-supervised monocular depth estimation. In *Proceedings of the IEEE/CVF international conference on computer vision*, pp. 3828–3838, 2019.

Vitor Guizilini, Rares Ambrus, Sudeep Pillai, Allan Raventos, and Adrien Gaidon. 3d packing for self-supervised monocular depth estimation. In *Proceedings of the IEEE/CVF conference on computer vision and pattern recognition*, pp. 2485–2494, 2020.

Marti A. Hearst, Susan T Dumais, Edgar Osuna, John Platt, and Bernhard Scholkopf. Support vector machines. *IEEE Intelligent Systems and their applications*, 13(4):18–28, 1998.

Sunghoon Im, Hae-Gon Jeon, Stephen Lin, and In So Kweon. Dpsnet: End-to-end deep plane sweep stereo. *arXiv preprint arXiv:1905.00538*, 2019.

Prannay Khosla, Piotr Teterwak, Chen Wang, Aaron Sarna, Yonglong Tian, Phillip Isola, Aaron Maschinot, Ce Liu, and Dilip Krishnan. Supervised contrastive learning. *NeurIPS*, 33:18661–18673, 2020.

Diederik P Kingma and Jimmy Ba. Adam: A method for stochastic optimization. *arXiv preprint arXiv:1412.6980*, 2014.

Lingdong Kong, Shaoyuan Xie, Hanjiang Hu, Lai Xing Ng, Benoit Cottereau, and Wei Tsang Ooi. Robodepth: Robust out-of-distribution depth estimation under corruptions. *Advances in Neural Information Processing Systems*, 36, 2024.

Balaji Lakshminarayanan, Alexander Pritzel, and Charles Blundell. Simple and scalable predictive uncertainty estimation using deep ensembles. *Advances in neural information processing systems*, 30, 2017.

Jin Han Lee, Myung-Kyu Han, Dong Wook Ko, and Il Hong Suh. From big to small: Multi-scale local planar guidance for monocular depth estimation. *arXiv preprint arXiv:1907.10326*, 2019.

Xiaoxiao Long, Lingjie Liu, Wei Li, Christian Theobalt, and Wenping Wang. Multi-view depth estimation using epipolar spatio-temporal networks. In *Proceedings of the IEEE/CVF Conference on Computer Vision and Pattern Recognition*, pp. 8258–8267, 2021.

Xiaoyang Lyu, Liang Liu, Mengmeng Wang, Xin Kong, Lina Liu, Yong Liu, Xinxin Chen, and Yi Yuan. Hr-depth: High resolution self-supervised monocular depth estimation. In *Proceedings of the AAAI Conference on Artificial Intelligence*, volume 35, pp. 2294–2301, 2021.

Matthew Matl. Pyrender. `https://github.com/mmatl/pyrender`, 2019.

Zak Murez, Tarrence Van As, James Bartolozzi, Ayan Sinha, Vijay Badrinarayanan, and Andrew Rabinovich. Atlas: End-to-end 3d scene reconstruction from posed images. In *Computer Vision–ECCV 2020: 16th European Conference, Glasgow, UK, August 23–28, 2020, Proceedings, Part VII 16*, pp. 414–431. Springer, 2020.

Richard A Newcombe, Shahram Izadi, Otmar Hilliges, David Molyneaux, David Kim, Andrew J Davison, Pushmeet Kohi, Jamie Shotton, Steve Hodges, and Andrew Fitzgibbon. Kinectfusion: Real-time dense surface mapping and tracking. In *2011 10th IEEE international symposium on mixed and augmented reality*, pp. 127–136. Ieee, 2011.

Matteo Poggi, Filippo Aleotti, Fabio Tosi, and Stefano Mattoccia. On the uncertainty of self-supervised monocular depth estimation. In *Proceedings of the IEEE/CVF Conference on Computer Vision and Pattern Recognition*, pp. 3227–3237, 2020.

Pierluigi Zama Ramirez, Alex Costanzino, Fabio Tosi, Matteo Poggi, Samuele Salti, Stefano Mattoccia, and Luigi Di Stefano. Booster: a benchmark for depth from images of specular and transparent surfaces. *IEEE Transactions on Pattern Analysis and Machine Intelligence*, 2023.

Kieran Saunders, George Vogiatzis, and Luis J Manso. Self-supervised monocular depth estimation: Let's talk about the weather. In *Proceedings of the IEEE/CVF International Conference on Computer Vision*, pp. 8907–8917, 2023.

Florian Schroff, Dmitry Kalenichenko, and James Philbin. Facenet: A unified embedding for face recognition and clustering. In *Proceedings of the IEEE conference on computer vision and pattern recognition*, pp. 815–823, 2015.

Xuepeng Shi, Georgi Dikov, Gerhard Reitmayr, Tae-Kyun Kim, and Mohsen Ghafoorian. 3d distillation: Improving self-supervised monocular depth estimation on reflective surfaces. In *Proceedings of the IEEE/CVF International Conference on Computer Vision*, pp. 9133–9143, 2023.

Jamie Shotton, Ben Glocker, Christopher Zach, Shahram Izadi, Antonio Criminisi, and Andrew Fitzgibbon. Scene coordinate regression forests for camera relocalization in rgb-d images. In *Proceedings of the IEEE conference on computer vision and pattern recognition*, pp. 2930–2937, 2013.

Adrian Spurr, Aneesh Dahiya, Xi Wang, Xucong Zhang, and Otmar Hilliges. Self-supervised 3d hand pose estimation from monocular rgb via contrastive learning. In *ICCV*, pp. 11230–11239, 2021.

Yaoming Wang, Yangzhou Jiang, Jin Li, Bingbing Ni, Wenrui Dai, Chenglin Li, Hongkai Xiong, and Teng Li. Contrastive regression for domain adaptation on gaze estimation. In *CVPR*, pp. 19376–19385, 2022.

Zhou Wang, Alan C Bovik, Hamid R Sheikh, and Eero P Simoncelli. Image quality assessment: from error visibility to structural similarity. *IEEE transactions on image processing*, 13(4):600–612, 2004.

Kaiwen Zha, Peng Cao, Jeany Son, Yuzhe Yang, and Dina Katabi. Rank-n-contrast: Learning continuous representations for regression. *Advances in Neural Information Processing Systems*, 36, 2024.

Chaoqiang Zhao, Youmin Zhang, Matteo Poggi, Fabio Tosi, Xianda Guo, Zheng Zhu, Guan Huang, Yang Tang, and Stefano Mattoccia. Monovit: Self-supervised monocular depth estimation with a vision transformer. In *2022 International Conference on 3D Vision (3DV)*, pp. 668–678. IEEE, 2022.

Hang Zhou, David Greenwood, and Sarah Taylor. Self-supervised monocular depth estimation with internal feature fusion. *arXiv preprint arXiv:2110.09482*, 2021.

Tinghui Zhou, Matthew Brown, Noah Snavely, and David G Lowe. Unsupervised learning of depth and ego-motion from video. In *Proceedings of the IEEE conference on computer vision and pattern recognition*, pp. 1851–1858, 2017.

Xiaowei Zhou, Haoyu Guo, Sida Peng, Yuxi Xiao, Haotong Lin, Qianqian Wang, Guofeng Zhang, and Hujun Bao. Neural 3d scene reconstruction with indoor planar priors. *IEEE Transactions on Pattern Analysis and Machine Intelligence*, 2024.

A More Detailed Experimental Setups

As aforementioned in the main manuscripts, we follow all training details and experimental setups mentioned in 3D Distillation (Shi et al., 2023). We train all models with the reflection triplet split proposed by 3D Distillation for 41 epochs through the Adam optimizer (Kingma & Ba, 2014) with an image resolution of 384×288, implemented in PyTorch. The training batch sizes of the Monodepth2 (Godard et al., 2019), HRDepth (Lyu et al., 2021), and MonoViT (Zhao et al., 2022) are $\{12, 12, 8\}$, respectively. The initial learning rate is 10^{-4}, and we adopt the multi-step learning rate scheduler that decays the learning rate by $\gamma = 0.1$ once the number of epochs reaches one of the milestones $[26, 36]$. Moreover, with 3D Distillation, the pose between cameras is ground truth during training, and the minimum and maximum depths used for training and evaluation are 0.1m and 10m. In our evaluation, we do not apply post-processing techniques such as averaging the estimates of both the flipped and original images or using median scaling.

Table 4: Main results on the ScanNet-Original Test and Validation sets.

Backbone	Training Scheme	Method	ScanNet-Original Test Set						
			Abs Rel ↓	Sq Rel ↓	RMSE ↓	RMSE log ↓	$\delta < 1.25$ ↑	$\delta < 1.25^2$ ↑	$\delta < 1.25^3$ ↑
Monodepth2	End-to-End	Self-Supervised	0.189	0.116	0.407	**0.217**	**0.731**	0.921	0.974
		Ours	**0.185**	**0.109**	**0.405**	**0.217**	0.730	**0.923**	**0.975**
	Multi-Stage	Self-Teaching	0.184	0.109	0.392	0.210	0.742	0.925	0.976
		3D Distillation	0.181	0.105	0.388	0.208	**0.746**	0.927	0.976
		Ours†	**0.175**	**0.098**	**0.385**	**0.206**	**0.746**	**0.930**	**0.979**
HRDepth	End-to-End	Self-Supervised	**0.184**	0.111	0.399	**0.212**	**0.739**	0.925	0.976
		Ours	0.186	**0.106**	**0.397**	0.213	0.735	**0.927**	**0.977**
	Multi-Stage	Self-Teaching	0.178	0.102	0.381	0.204	0.752	0.931	0.979
		3D Distillation	0.176	0.098	0.378	**0.202**	0.754	0.932	0.979
		Ours†	**0.173**	**0.096**	**0.375**	**0.202**	**0.755**	**0.934**	**0.980**
MonoViT	End-to-End	Self-Supervised	**0.154**	0.082	**0.343**	**0.182**	**0.801**	**0.948**	**0.984**
		Ours	0.155	**0.081**	0.345	0.185	0.795	0.945	**0.984**
	Multi-Stage	Self-Teaching	0.152	0.081	0.329	0.177	0.811	0.948	0.983
		3D Distillation	**0.149**	**0.075**	**0.324**	**0.174**	**0.812**	**0.949**	**0.985**
		Ours†	**0.149**	**0.075**	0.335	0.179	0.805	**0.949**	0.980
Backbone	Training Scheme	Method	ScanNet-Original Val. Set						
			Abs Rel ↓	Sq Rel ↓	RMSE ↓	RMSE log ↓	$\delta < 1.25$ ↑	$\delta < 1.25^2$ ↑	$\delta < 1.25^3$ ↑
Monodepth2	End-to-End	Self-Supervised	0.167	0.100	0.385	0.203	0.764	0.935	0.981
		Ours	**0.162**	**0.090**	**0.378**	**0.201**	**0.765**	**0.937**	**0.983**
	Multi-Stage	Self-Teaching	0.160	0.090	0.365	0.193	0.780	0.941	0.983
		3D Distillation	0.157	0.083	**0.357**	**0.190**	0.782	0.943	**0.985**
		Ours†	**0.153**	**0.080**	0.358	**0.190**	**0.783**	**0.944**	**0.985**
HRDepth	End-to-End	Self-Supervised	0.166	0.100	0.381	0.200	0.771	0.937	0.982
		Ours	**0.160**	**0.089**	**0.373**	**0.197**	**0.772**	**0.941**	**0.984**
	Multi-Stage	Self-Teaching	0.159	0.090	0.360	0.190	0.785	0.943	0.984
		3D Distillation	0.154	0.080	**0.349**	**0.186**	0.788	0.945	0.986
		Ours†	**0.151**	**0.078**	0.350	**0.186**	**0.790**	**0.948**	**0.987**
MonoViT	End-to-End	Self-Supervised	0.138	0.077	0.331	**0.171**	**0.831**	0.955	0.986
		Ours	**0.137**	**0.069**	**0.328**	0.172	0.826	**0.958**	**0.989**
	Multi-Stage	Self-Teaching	0.133	0.071	0.314	0.163	0.844	0.959	0.988
		3D Distillation	**0.128**	**0.060**	**0.296**	**0.157**	**0.846**	**0.962**	**0.990**
		Ours†	0.129	0.062	0.310	0.163	0.840	0.961	**0.990**

B Evaluations on ScanNet Dataset

To demonstrate the generalizability of our proposed method, we conduct the experiment on several ScanNet (Dai et al., 2017) splits denoted as ScanNet-Original $\{$Test, Val.$\}$ sets and ScanNet-Robust Test set following Shi et al. (2023) and Fu et al. (2018); Bae et al. (2022), respectively. ScanNet-Original sets include both reflective and non-reflective surfaces, it is well-suited to evaluate the impact of reflective surfaces on training comprehensively. In addition, the ScanNet-Robust test set was used to measure the generalization performance of Monocular Depth Estimation in the Robust Vision Challenge 2018 (Geiger et al., 2018), as it is small-scale but suitable for evaluating generalization performance.

B.1 Evaluation on ScanNet-Original Sets

Table 4 summarizes the quantitative evaluation results of the ScanNet-Original sets. We achieve steady performance improvement across most metrics for all backbone models in the end-to-end training scheme, suggesting that the proposed method minimizes the influence of reflective surfaces, which contributes to the general depth estimation performance improvement.

Furthermore, Our multi-stage training scheme (*i.e.*, *Ours*†) dramatically elevates performance across various depth estimation models. For Monodepth2, *Ours*† achieves a remarkable average increase of 5.28% on the test set and 6.52% on the validation set across all metrics. HRDepth reaps substantial benefits, with improvements of 4.83% on the test set and 7.19% on the validation set. Likewise, MonoViT consistently gains, with enhancements of 2.28% on the test set and 5.59% on the validation set. When benchmarked against 3D Distillation (Shi et al., 2023), *Ours*† provides an enhanced performance for Monodepth2, showing an average increase of 1.76% on the test set and 0.87% on the validation set. HRDepth also gains an average of 0.71% on the test set and 0.69% on the validation set. However, for MonoViT, *Ours*† shows a slight decline, with decreases of 1.09% on the test set and 1.92% on the validation set compared to 3D Distillation.

Table 5: Main results on the ScanNet-Robust Test set.

Backbone	Method	ScanNet-Robust Test Set						
		Abs Rel ↓	Sq Rel ↓	RMSE ↓	RMSE log ↓	$\delta < 1.25 \uparrow$	$\delta < 1.25^2 \uparrow$	$\delta < 1.25^3 \uparrow$
Monodepth2	Self-Supervised	0.193	0.118	0.395	0.219	0.729	0.921	0.973
	Ours	0.186	0.107	0.388	0.216	0.729	0.926	0.976
	Ours†	**0.179**	**0.099**	**0.371**	**0.207**	**0.744**	**0.930**	**0.978**
HRDepth	Self-Supervised	0.190	0.112	0.387	0.216	0.729	0.924	0.976
	Ours	0.188	0.107	0.384	0.215	0.731	0.926	0.976
	Ours†	**0.177**	**0.095**	**0.362**	**0.203**	**0.750**	**0.935**	**0.979**
MonoViT	Self-Supervised	0.158	0.082	0.328	0.181	0.799	0.948	0.984
	Ours	0.155	0.078	0.327	0.183	0.798	0.949	0.985
	Ours†	**0.150**	**0.073**	**0.319**	**0.178**	**0.806**	**0.952**	**0.986**

B.2 Evaluation on ScanNet-Robust Test Set

Table 5 summarizes the quantitative evaluation results of the ScanNet-Robust test set. Due to the 3D-distillation baselines (Shi et al., 2023) did not release the source code, and the reported performance on this split not existing, we compare the models trained by our methods to the self-supervised methods across three backbones, similar to previous experiments. As depicted in Table 5, our proposed methods (*i.e.*, *Ours*, *Ours*†) achieve significant performance gains for all evaluation metrics and all backbones, consistently. Specifically, for Monodepth2, *Ours* and *Ours*† demonstrate an average performance improvement of 2.42% and 5.49%, respectively, across all metrics. Similarly, for HRDepth, *Ours* showed an average improvement of 1.03%, and *Ours*† achieved a 5.55% increase in performance across all metrics. In the case of MonoViT, *Ours* resulted in an average performance improvement of 0.87%, and *Ours*† achieved a 3.13% improvement across all metrics. The consistent improvements across all metrics for Monodepth2, HRDepth, and MonoViT indicate that our methods effectively mitigate the risk of erroneous learning induced by reflective surfaces.

C Qualitative Results on 7-Scenes and Booster Datasets

We provide additional qualitative results of the proposed methods denoted as *Ours* and *Ours*† as discussed in Table 3 of the main manuscript, utilizing the 7-Scenes (Shotton et al., 2013) and Booster (Ramirez et al., 2023) datasets. In Figure 4, we showcase the predicted depth and error map of the Monodepth2 trained by self-supervised, $\mathcal{L}_{tri}$, and $\mathcal{L}_{rkd}$. Our methods alleviate the black-hole effect on specular highlight regions while preserving high-frequency details on non-reflective areas. As demonstrated by the qualitative evaluation of the 7-Scenes dataset, our proposed methods exhibit robustness to reflective surfaces and impressive performance in preserving details on non-reflective surfaces in other indoor scenes that are similar to the training environment.

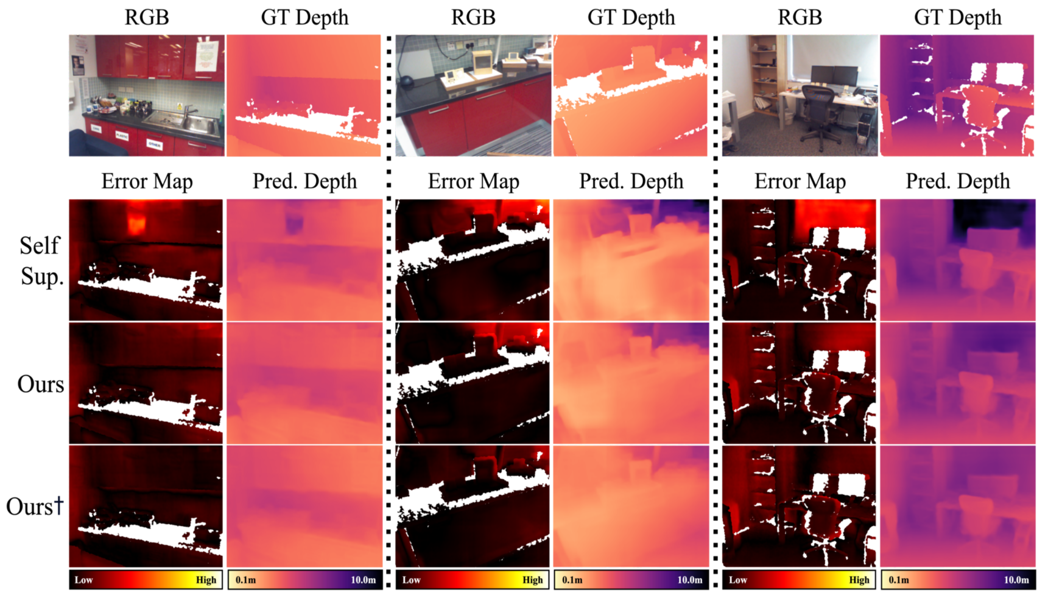

(a) Qualitative results of the proposed methods on the 7-Scenes dataset.

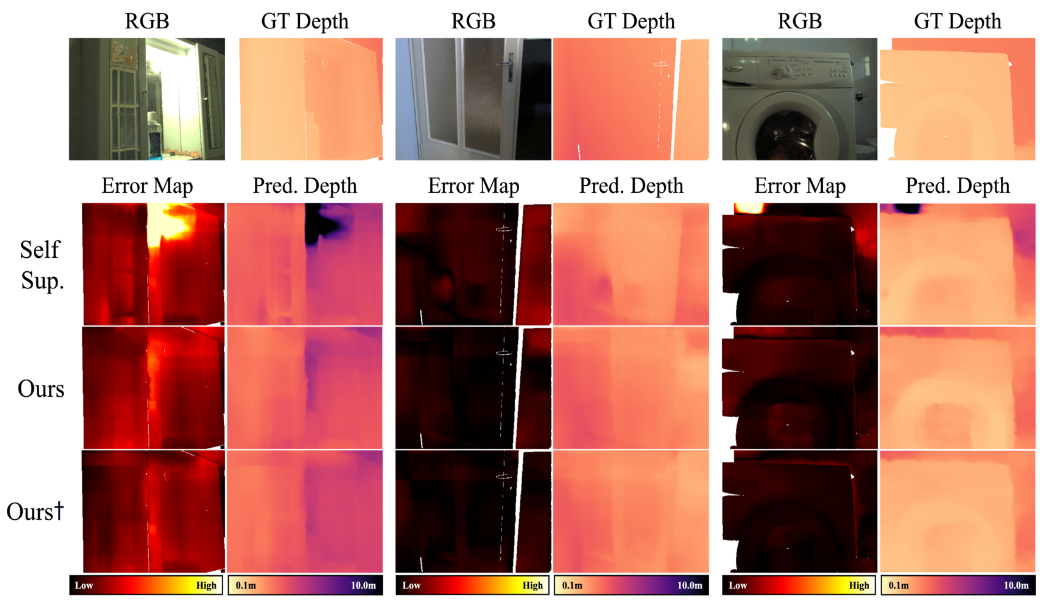

(b) Qualitative results of the proposed methods on the Booster dataset.

Figure 4: Qualitative results of the proposed methods on the 7-scenes and Booster datasets. Note that the error map represents the absolute difference between prediction and ground truth depth, normalized to between 0 and 255.

Table 6: Evaluation results on the ScanNet-Reflection Validation and ScanNet-NoReflection Validation sets. w.r.t. reflective region mask M_r.

Backbone	Method	ScanNet-Reflection Validation Set				ScanNet-NoReflection Validation Set			
		Abs Rel ↓	Sq Rel ↓	RMSE ↓	$\delta < 1.25^3$ ↑	Abs Rel ↓	Sq Rel ↓	RMSE ↓	$\delta < 1.25^3$ ↑
Monodepth2	$M_r = 0$	0.206	0.227	0.584	0.961	0.169	0.100	**0.395**	0.979
	$M_r = 1$	0.170	0.132	0.505	0.979	0.171	0.099	0.402	0.978
	Ours	**0.166**	**0.125**	**0.492**	**0.981**	**0.168**	**0.095**	**0.395**	**0.980**
HRDepth	$M_r = 0$	0.213	0.244	0.605	0.961	0.169	0.102	**0.388**	**0.980**
	$M_r = 1$	0.184	0.167	0.564	0.965	0.179	0.113	0.433	0.968
	Ours	**0.167**	**0.127**	**0.496**	**0.982**	**0.167**	**0.096**	0.389	0.979
MonoViT	$M_r = 0$	0.179	0.206	0.557	0.963	**0.140**	0.074	**0.333**	0.984
	$M_r = 1$	0.155	0.151	0.527	0.971	0.168	0.112	0.420	0.954
	Ours	**0.139**	**0.107**	**0.452**	**0.984**	0.141	**0.072**	0.338	**0.987**

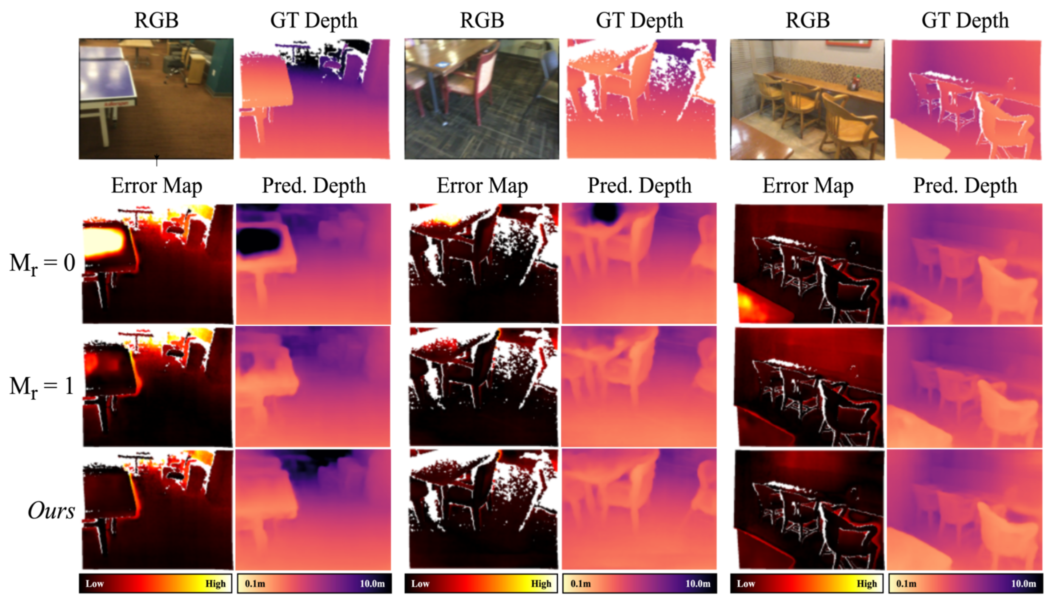

Figure 5: Qualitative results of the proposed methods w.r.t. reflective region mask M_r.

D IMPACT OF THE REFLECTION-AWARE TRIPLET MINING LOSS W.R.T. REFLECTIVE REGION LOCALIZATION

As aforementioned in the main manuscript, the proposed reflection-aware triplet mining loss is applied to reflective regions, thus preserving performance in non-reflective regions. To validate this claim, we conduct an experiment to evaluate the impact of varying the reflection mask M_r with three configurations as follows:

1. $M_r = 0$: This configuration exactly corresponds to the traditional self-supervised method without the triplet mining loss.
2. $M_r = 1$: In this configuration, the triplet loss is applied to both reflective and non-reflective regions of the image.
3. *Ours*: This configuration leverages M_r, which is calculated through Equation 8 in the main manuscript, to selectively regulates the reflective regions.

As shown in Table 6, the results demonstrate that *Ours* significantly improves performance on reflective datasets while maintaining comparable performance on non-reflective regions when compared to the first configuration (denoted as $M_r = 0$). On the other hand, applying the triplet mining loss across all regions ($M_r = 1$) led to some performance improvement in reflective regions but resulted in a notable drop in performance in non-reflective regions compared to other configurations. These findings verify that the proposed reflection-aware triplet mining loss effectively identifies reflective regions and applies the triplet loss selectively, thereby preserving the performance in non-reflective regions.

E LIMITATIONS

Despite the promising results, our study has several limitations. One major limitation is that the proposed method cannot handle transparent or mirror (ToM) objects. Secondly, a few cases do not satisfy the assumption of Equation 8 of the manuscript (*e.g.*, surfaces including multiple reflection lobes). Lastly, similar to 3D distillation (Shi et al., 2023), the conducted experiments assume that the ground truth camera pose is known during training.